Model Predictive Control With Stability Guarantee for Second-Order DC/DC Converters

Alejandro Garcés-Ruiz, *Senior Member, IEEE*, Sebastián Riffo, Catalina González-Castaño, and Carlos Restrepo

***Abstract*—This article proposes a continuous-control-set model-predictive control (CCS-MPC) designed explicitly for second-order dc/dc converters, such as the boost, buck, buck–boost, and noninverting buck–boost converters. These converters share a bilinear dynamic structure that allows designing a generalized control. In contradistinction to the conventional finite-control-set approach, the proposed control uses a pulsewidth modulation that allows a continuous control set with constant switching frequency. The modulation index's saturation is considered an inequality constraint in the optimization model. The proposed control guarantees stability in the sense of Lyapunov. This property is proven by using the passive structure of these converters. Experimental results on the four converters mentioned previously show the superior performance of the proposed control in terms of robustness, offset, computation time in the central processing unit, and, of course, stability.**

***Index Terms*—Bilinear systems, boost converter, buck converter, buck–boost converter, continuous-control-set model-predictive control (CCS-MPC), dc–dc converters, Lyapunov stability, model-predictive control (MPC), noninverting buck–boost converter, one-step MPC.**

Manuscript received 18 October 2022; revised 14 March 2023; accepted 31 May 2023. Date of publication 12 June 2023; date of current version 18 December 2023. This work was supported in part by the Agencia Nacional de Investigación y Desarrollo (ANID) under Grants ANID/FONDECYT 1231015, in part by the Millennium Institute on Green Ammonia as Energy Vector MIGA through ANID/Millennium Science Initiative Program under Grant ICN2021_023, and in part by the Centre for Multidisciplinary Research on Smart and Sustainable Energy Technologies for Sub-Antarctic Regions under Climate Crisis ANID/ATE220023 and SERC Chile ANID/FONDAP/1522A0006. *(Corresponding author: Carlos Restrepo.)*

Alejandro Garcés-Ruiz is with the Department of Electric Power Engineering, Universidad Tecnológica de Pereira, Pereira 660003, Colombia (e-mail: alejandro.garces@utp.edu.co).

Sebastián Riffo is with the Department of Electrical Engineering, Universidad de Talca, Curicó 3340000, Chile (e-mail: sebastian.riffo@utalca.cl).

Catalina González-Castaño is with the Centro de Transformación Energética, Facultad de Ingeniería, Universidad Andres Bello, Santiago 7500971, Chile, and also with the Assistant Investigator MIGA 7820436, Chile (e-mail: catalina.gonzalez@unab.cl).

Carlos Restrepo is with the Department of Electrical Engineering, Universidad de Talca, Curicó 3340000, Chile, and also with the Principal investigator MIGA 7820436, Chile (e-mail: crestrepo@utalca.cl).

Color versions of one or more figures in this article are available at https://doi.org/10.1109/TIE.2023.3283706.

Digital Object Identifier 10.1109/TIE.2023.3283706

I. Introduction

MODEL-PREDICTIVE control (MPC) has become popular in industrial electronic applications due to its advantages in terms of performance and its capability to introduce constraints effortlessly [1], [2], [3]. In total, two main approaches exist for MPC in power electronic applications [4], [5]: finite-control-set MPC (FCS-MPC) and continuous-control-set MPC (CCS-MPC). In FCS-MPC, the control signals act directly on a finite set of switching states, whereas they are continuous-time signals, sent to a pulsewidth modulator, in the CCS-MPC [6].

Despite its simple implementation and good performance, the FCS-MPC has some drawbacks, such as a nonconstant switching frequency and high sampling frequency, making the microcontroller works near its operation limit [7]. Additional calculations are required to obtain an FCS-MPC with constant switching frequency [8], [9]. Hence, CCS-MPC may have advantages since a pulsewidth modulation (PWM) maintains a constant switching frequency [10], [11]. However, the model is more complex since the saturation of the modulation index must be included as an inequality constraint.

A comparison between FCS-MPC and CCS-MPC for speed control of induction motors was presented in [12]. CCS-MPC presented less computational complexity and low current ripple. Heightened performance was also obtained for the permanent magnet synchronous generator [13], six-phase drivers [14] dc/ac converters [15], [16], [17], [18], and matrix converters [19]. Far fewer articles were found about CCS-MPC for dc/dc converters [11], [20], [21], [22].

Stability can be ensured in MPC by imposing long horizons, terminal constraints, or penalization in the final step [23]. This approach is helpful in applications where the dynamic is slow, e.g., chemical applications. However, power electronics applications use an ad-hoc MPC with short horizons and simplified optimization models that can be implemented in real time. In [24], an MPC for motor drives was presented. A stability criterion was included in the control, but it was not formally demonstrated. A similar approach was presented in [25], where the stability was enhanced but not ensured. Therefore, the primary question of how to guarantee stability in MPC for power electronics applications remained open [26].

Achieving offset-free tracking for dc–dc converters is another aspect closely related to the stability problem. Hence, a hybrid MPC was proposed in [3]. An offset-free MPC was proposed for a dc/dc buck converter with constant power loads. It guaranteed

stability but with variable frequency and was implemented with a high-order sliding mode observer to estimate the future tracking error. Another hybrid MPC controller was proposed in [27], where averaged and continuous time models were implemented for a dc/dc boost converter to maintain stability in systems with constant power loads. Although the method performs well, it works with a variable frequency. Thus, to the best of the authors' knowledge, there is no MPC that considers continuous control set, constant frequency, and guarantee of stability for second-order converters.

This article fills this gap by proposing a new type of continuous-set MPC with a guarantee of stability. Our control is oriented to bilinear second-order converters. These converters include the buck, boost, buck–boost, and noninverting buck–boost, among others. The theory is general enough to be used in any converter with the same bilinear structure. The control combines the advantages of MPC in terms of performance, constraints qualifications, and the stability properties of passivity-based control. The contributions are threefold, and are given as follows.

1) The proposed control guarantees stability in the sense of Lyapunov and is general for any second-order converter. This theoretical result was tested experimentally in four commonly known converters: the buck, boost, buck–boost and noninverting buck–boost. However, the control is general for any converter with the same mathematical structure.
2) The proposed control has a more straightforward implementation than other classical predictive techniques. This aspect is evaluated by the CPU utilization of the algorithm, compared with the FCS-MPC.
3) The proposed control operates at a constant frequency. Besides, it is more robust than FCS-MPC and conventional proportional–integral (PI) controls.

The rest of this article is organized as follows. Section II shows the model for second-order dc/dc converters, their bilinear structure, and the proposed control. Next, the stability analysis is given in Section III. After that, experimental results are presented in Section IV. Finally, Section V concludes this article and presents future works.

II. CCS-MPC for Second-Order DC/DC Converters

A. Bilinear Structure of DC/DC Converters

We consider dc/dc power electronic converters, such as the buck, boost, buck–boost, and the noninverting buck–boost, given in Table I (see [28] for more details about modeling dc/dc converters). These converters share a similar structure; namely, they are representable as a discrete-time bilinear system, given as follows:

$$x_{t+1} = Ax_t + u_t\psi(x_t) \tag{1}$$

where t symbolizes the discrete time, state variables are given by a vector $x \in \mathbb{R}^2$ that represents input current and output voltage, e.g., $x = (i_0, v_L)$, and a single input u represents the modulation index; this model includes a linear part represented by a matrix

TABLE I
EXAMPLES OF SECOND-ORDER DC/DC CONVERTERS

Converter	A	B	b
Buck	$\begin{bmatrix} 1 & \frac{\tau}{L} \\ \frac{\tau}{C} & 1 - \frac{\tau}{R_L C} \end{bmatrix}$	$\begin{bmatrix} 0 & 0 \\ 0 & 0 \end{bmatrix}$	$\begin{bmatrix} \frac{TV_g}{L} \\ 0 \end{bmatrix}$
Boost	$\begin{bmatrix} 1 & \frac{\tau}{L} \\ \frac{\tau}{C} & 1 - \frac{\tau}{R_L C} \end{bmatrix}$	$\begin{bmatrix} 0 & \frac{\tau}{L} \\ \frac{\tau}{C} & 0 \end{bmatrix}$	$\begin{bmatrix} 0 \\ 0 \end{bmatrix}$
Buck–Boost	$\begin{bmatrix} 1 & \frac{\tau}{L} \\ \frac{T\tau}{C} & 1 - \frac{\tau}{R_L C} \end{bmatrix}$	$\begin{bmatrix} 0 & \frac{\tau}{L} \\ \frac{\tau}{C} & 0 \end{bmatrix}$	$\begin{bmatrix} \frac{TV_g}{L} \\ 0 \end{bmatrix}$
Non inverting Buck–Boost	$\begin{bmatrix} 1 & \frac{\tau}{L} \\ \frac{\tau}{C} & 1 - \frac{\tau}{R_L C} \end{bmatrix}$	$\begin{bmatrix} 0 & \frac{\tau}{L} \\ \frac{\tau}{C} & 0 \end{bmatrix}$	$\begin{bmatrix} \frac{TV_g}{L} \\ 0 \end{bmatrix}$

$A \in \mathbb{R}^{2\times 2}$ and a nonlinear part that includes the product of u and $\psi : \mathbb{R}^2 \to \mathbb{R}$. The latter is given by the following affine function:

$$\psi(x_t) = Bx_t + b$$

with $B \in \mathbb{R}^{2\times 2}$ and $b \in \mathbb{R}^2$. Parameters A, B, and b are given in Table I for each of the converters considered, where τ is the discretization time. Other parameters can be interpreted directly from the corresponding figures. The following assumptions are considered.

Assumption 1: There exists an admissible equilibrium point in $x = 0$ and $u = 0$. Any other admissible equilibrium point $(\tilde{x}, \tilde{u})$ can be translated to (0,0) by a change of variables.

Assumption 2: There exists a matrix $Q \in \mathbb{R}^{n\times n}$ such that $Q = Q^\top \succ 0$, and $Q \succeq A^\top QA$.

Assumption 1 guarantees the existence of the equilibrium and the possibility to change variables to translate this equilibrium to the point (0,0). Assumption 2 is required for two reasons: first, Q must be positive definite in order to define a convex quadratic optimization that can be minimized; the second condition allows defining a passive dynamic system in which stability can be guaranteed, as given in Section III.

B. Proposed Control

The control is designed according to the following optimization model:

$$\begin{aligned} \min\ & \frac{1}{2}x_{t+1}^\top Q x_{t+1} + \frac{1}{2}\rho u_t^2 \\ & x_{t+1} = Ax_t + u_t\psi(x_t) \\ & \psi(x_t) = Bx_t + b \\ & u_t \in \mathcal{U} \end{aligned} \tag{2}$$

with $Q = Q^\top \succ 0$, $\rho > 0$; $\mathcal{U}$ is the following compact set:

$$\mathcal{U} = \{u \in \mathbb{R} :\ \underline{u} \le u \le \bar{u}\}$$

with $\bar{u} \ge 0$ and $\underline{u} \le 0$. These limits correspond to the saturations of modulation index. It is imperative to consider these limits, since the model may change under saturation.

We define the following Lagrangian function to solve the optimization problem:

$$\begin{aligned} \mathcal{L}(x_{t+1}, u_t, \lambda, \gamma_0, \gamma_1) &= \frac{1}{2}x_{t+1}^\top Q x_{t+1} + \frac{1}{2}\rho u_t^2 \\ &+ \lambda^\top(x_{t+1} - Ax_t - u_t\psi_t) + \gamma_0(\underline{u} - u_t) + \gamma_1(u_t - \bar{u}) \end{aligned}$$

where λ are dual variables. The Karush–Kuhn–Tucker conditions are given as follows:

$$Qx_{t+1} + \lambda = 0 \tag{3}$$

$$\rho u_t - \lambda^\top\psi(x_t) - \gamma_0 + \gamma_1 = 0 \tag{4}$$

$$x_{t+1} - Ax_t - u_t\psi(x_t) - d = 0 \tag{5}$$

$$\gamma_0(\underline{u} - u_t) = 0 \tag{6}$$

$$\gamma_1(u_t - \bar{u}) = 0 \tag{7}$$

$$\gamma_0 \ge 0 \tag{8}$$

$$\gamma_1 \ge 0 \tag{9}$$

$$u_t \ge \underline{u} \tag{10}$$

$$u_t \le \bar{u}. \tag{11}$$

We combine (3), (4), and (5) into a single equation for the input u_t

$$u_t = \frac{-(Ax_t)^\top Q\psi(x_t) + \gamma_0 - \gamma_1}{\rho + \psi(x_t)^\top Q\psi(x_t)}.$$

We can identify three possible outcomes: if $\underline{u} < u < \bar{u}$, then $\lambda_0 = 0$ and $\lambda_1 = 0$ in view of (6) and (7); if $u_t = \underline{u}$, then $\lambda_0 > 0$ due to (8) and (10); finally, if $u_t = \bar{u}$, then $\lambda_1 > 0$ due to (9) and (11). These three outcomes can be represented by the projection operator, given as follows:

$$\text{proj}_{\mathcal{U}}(u) = \left\{ \begin{array}{cc} \underline{u} & \text{if } u < \underline{u} \\ u & \text{if } \underline{u} \le u \le \bar{u} \\ \bar{u} & \text{if } u > \bar{u} \end{array} \right\}.$$

Therefore, the control has the following solution:

$$u_t = \text{proj}_{\mathcal{U}}\left(-\frac{(Ax_t)^\top Q\psi(x_t)}{\rho + \psi(x_t)^\top Q\psi(x_t)}\right). \tag{12}$$

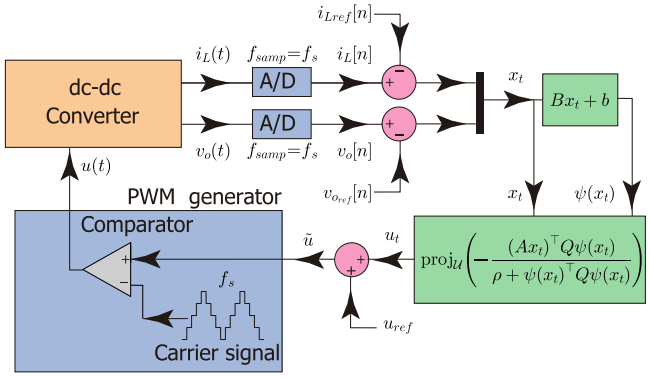

Fig. 1. Block diagram for the proposed continuous-set MPC.

The practical implementation of this control is depicted in Fig. 1. It receives measurements of the states and the desired equilibrium point. Then, (12) is used to calculate the modulation index, which, in turn, is used by the PWM. Commutation frequency is constant according to the PWM. This frequency might be higher or equal to the frequency of the control. Notice that (12) is quite simple for practical implementations, even in low-cost boards.

III. Stability Analysis

Stability is usually imposed in MPCs using long time horizons and penalization functions in the last stage. However, a CCS-MPC, as the one presented here, requires a short horizon due to the fast dynamics of dc/dc converters. The existence and uniqueness of this control can be guaranteed, as given in the following.

Lemma 1: Model (2) has a well-defined solution, given by (12). This solution corresponds to the global optimum, and it is unique.

Proof: Assumption 1 guarantees the existence of the equilibrium point; besides, $\rho + \psi(x_t)^\top Q\psi(x_t) > 0\ \forall x_t$. Hence, the control is well defined for any x. The complementary slackness conditions and the inequality constraints can be incorporated into the control as (12). Uniqueness of the solution and global optimum come from the fact that the problem is convex, and the objective function is strictly convex for $Q \succ 0$. ■

Remark 1: Well defined indicates that a discontinuity, or division by zero, will never occur in the microcontroller. Notice that (12) is well defined even if Q were singular (i.e., positive semidefinite but not positive definite), since $\rho > 0$. However, in that case, the objective function is not strictly convex and uniqueness cannot be guaranteed. The optimum is still global.

Second-order converters have a passive structure, common in power electronic converters. Let us formally define this concept.

Definition 1: A discrete-time system is said to be passive if there exists a nonnegative $V : \mathbb{R}^n \to \mathbb{R}$ with $V(0) = 0$, called a storage function, such that the dissipation inequality

$$V(x_{t+1}) - V(x_t) \le y_t u_t$$

holds for any input vector u_t and output vector y_t.

Lemma 2: Suppose Assumptions 1 and 2 hold. Then, (1) is a passive system with a storage function

$$V(x) = x^\top Q x$$

and output

$$y_t = 2\psi(x_t)^\top Q A x_t + u\psi(x_t)^\top Q \psi(x_t).$$

Proof: Define $\psi_t = \psi(x_t)$; then, a straightforward computation shows that

$$\begin{aligned} V(x_{t+1}) - V(x_t) &= x_{t+1}^\top Q x_{t+1} - x_t^\top Q x_t \\ &= (Ax_t + u_t\psi_t)^\top Q (Ax_t + u_t\psi_t) \\ &= x_t^\top A^\top Q A x_t + 2u_t\psi_t^\top Q A x_t \\ &\quad + u_t^2 \psi_t^\top Q \psi_t - x_t^\top Q x_t \\ &\leq u_t \left(2\psi_t^\top Q A x_t + u_t \psi_t^\top Q \psi_t\right) \\ &\leq y_t u_t. \end{aligned}$$

Hence, the system is passive. ■

Lemma 3: Suppose that Assumptions 1 and 2 hold, the unforced dynamic system of (1) is stable.

Proof: Define a Lyapunov function $V(x) = x^\top Q x$. Then, we have the following:

$$V(x_{t+1}) - V(x_t) \leq 0$$

for $u_t = 0$. ■

This lemma shows a remarkable stability property of the systems studied in this article. The system is stable for $u = 0$. However, this property may be destroyed by the design of the control. Therefore, the control must be designed to maintain the structure.

Theorem 1: Consider the discrete-time affine nonlinear systems given by (1) and suppose it fulfills Assumptions 1 and 2. Then, the application of the MPC obtained by (2) is globally asymptotically stable.

Proof: Define $\mathcal{J} : \mathbb{R} \to \mathbb{R}$ as follows:

$$\mathcal{J}(u_t) = \frac{1}{2}\left(Ax_t + u_t\psi(x_t)\right)^\top Q \left(Ax_t + u_t\psi(x_t)\right) + \frac{1}{2}\rho u_t^2.$$

Then, (2) is equivalent to

$$\min \mathcal{J}(u_t) \quad \text{with} \quad u_t \in \mathcal{U}. \tag{13}$$

Notice that the gradient of $\mathcal{L}$ can be represented as a function of the passive output, given as follows:

$$\nabla_u \mathcal{J} = y_t + u_t(\rho + \psi_t^\top Q \psi_t).$$

Now, the Lagrangian function associated with (13) is

$$\mathcal{L}(u, \gamma_0, \gamma_1) = \mathcal{J}(u) + \gamma_0(\underline{u} - u) + \gamma_1(u - \bar{u})$$

where γ_0 and γ_1 are dual variables. The Karush–Kuhn–Tucker conditions are given as follows:

$$\begin{aligned} \nabla_u \mathcal{J} - \gamma_0 + \gamma_1 &= 0 \\ \gamma_0(\underline{u} - u) + \gamma_1(u - \bar{u}) &= 0 \\ \gamma_0 &\geq 0 \\ \gamma_1 &\geq 0 \\ u &\geq \underline{u} \\ u &\leq \bar{u}. \end{aligned}$$

Since $\underline{u} \leq 0$ and $\bar{u} \geq 0$, the last conditions imply the following:

$$0 \geq \gamma_0 \underline{u} - \gamma_1 \bar{u} = (\gamma_0 - \gamma_1)u.$$

Moreover, the first condition allows to represent the passive output as function of the dual variables, namely

$$y_t = -u_t(\rho + \psi_t^\top Q \psi_t) + (\gamma_0 - \gamma_1).$$

Multiplying by u_t and using the fact that the system is passive (Lemma 2), we have the following:

$$\begin{aligned} V(x_{t+1}) - V(x_t) &\leq y_t u_t \\ &= -u_t^2(\rho + \psi_t^\top Q \psi_t) + u_t(\gamma_0 - \gamma_1) \\ &\leq -u_t^2(\rho + \psi_t^\top Q \psi_t) < 0 \text{ for } u_t \neq 0. \end{aligned}$$

Here, we used the fact that $\rho > 0$ to conclude the proposed control is globally asymptotically stable. ■

Remark 2: Notice that the control is not only stable but globally asymptotically stable for any $\rho > 0$. This is a very strong result compared with previous approaches of CCS-MPC.

A. Selection of the Matrix Q

Different values of Q may be used as soon as it fulfills Assumption 2. The following convex optimization model with semidefinite constraints is proposed to calculate Q:

$$\begin{aligned} \min \quad & \|Q\| \\ & Q \succeq 0 \\ & Q - A^\top Q A \succeq 0 \\ & Q_{11} = 1 \end{aligned} \tag{14}$$

where $\|\cdot\|$ represents any matrix norm. On the other hand, ρ can have any positive value.

IV. Simulation and Experimental Results

The proposed CCS-MPC was validated on second-order dc/dc converters listed in Table I using a reconfigurable dc/dc converter. The experimental setup is shown in Fig. 2. Converters' parameters are given in Table II. A PLECS RT-box was used to implement the control and calculate the modulation index u. Parameters of the quadratic form Q were calculated using model (14) for each converter (see Table III). These models were implemented in CVX, a package for specifying and solving convex programs [29], [30]. Input penalization was $\rho = 0.05$ in all cases. These values are not unique. Any set of parameters for Q and ρ are suitable as long as they meet conditions of Theorem 1.

Fig. 3 shows simulated and experimental results for the buck converter. A change of reference was applied to evaluate performance and stability. This transient can be appreciated in the zoomed picture at the bottom of each figure. The voltage dynamic is slower than the current. However, tracking the reference

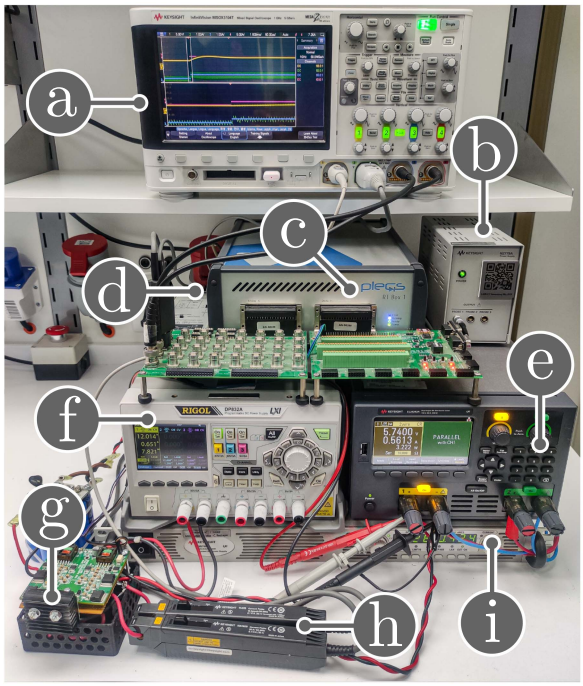

Fig. 2. Experimental setup. (a) Oscilloscope. (b) Current probe power supply. (c) RT-Box with analog and digital breakout boards. (d) Differential voltage probe. (e) DC electronic load. (f) MOSFET driver power supply. (g) Reconfigurable dc/dc converter. (h) Current probes. (i) Input voltage power supply.

TABLE II
SELECTED COMPONENTS FOR THE DC–DC CONVERTERS

Parameter	Component
Switching frequency f_s	100 kHz
MOSFETs S_1, S_2	Power MOSFET IRFB4510PBF
Diodes D_1, D_2	Schottky Power MBR60H100CTG
Inductor L	Wurth Elektronik 74435584700, 47 μH
Capacitor C	Multilayer Ceramic
	TDK C5750X7S2A106M230KB, 10 10 μF

TABLE III
PARAMETERS OF THE CONTROL

Converter	Input voltage	Load	Q
Buck	20 V	5Ω	$\begin{pmatrix} 1.000 & 0.087 \\ 0.087 & 1.88 \end{pmatrix}$
Boost	10 V	20Ω	$\begin{pmatrix} 1.000 & 0.024 \\ 0.024 & 2.09 \end{pmatrix}$
Buck–Boost	10 V	10Ω	$\begin{pmatrix} 1.000 & 0.047 \\ 0.047 & 2.015 \end{pmatrix}$
NI buck–boost	10 V	10Ω	$\begin{pmatrix} 1.000 & 0.047 \\ 0.047 & 2.015 \end{pmatrix}$

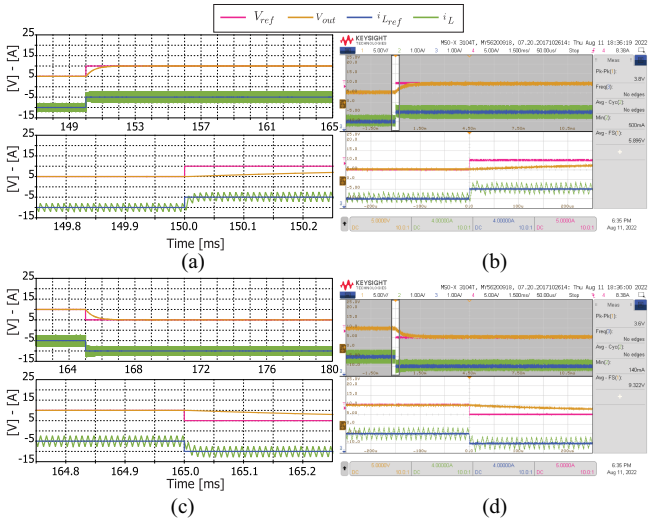

Fig. 3. (a), (c) Simulated and (b), (d) experimental dynamic responses of the buck converter with a load resistance R_L of 5 Ω while the duty cycle reference changes from: (a), (b) 0.25 to 0.5 and (c), (d) 0.5 to 0.25.

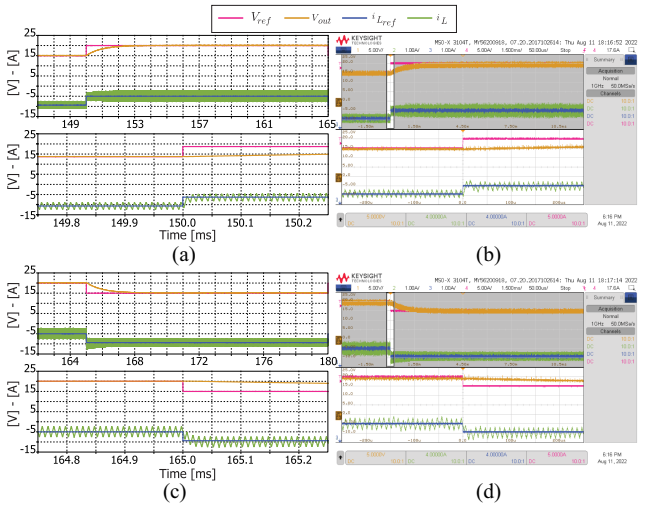

Fig. 4. (a), (c) Simulated and (b), (d) experimental dynamic responses of the boost converter with a load resistance R_L of 20 Ω while the duty cycle reference changes from: (a), (b) 0.33 to 0.5 and (c), (d) 0.5 to 0.33.

was fast, with a setting time of 1.5 ms. Simulated and experimental results for the boost converter are shown in Fig. 4, with a duty cycle reference change from 0.33 to 0.5 and vice versa. Inductor's current and capacitor's voltage accurately followed the references in both experimental and simulated results. Fig. 4 shows a fast inductor current tracking with a short setting time of 1.5 ms for the capacitor voltage.

Fig. 5 shows the performance of the proposed control considering the buck–boost converter. The simulated and experimental results show that the control achieves a very good tracking performance for the buck and boost modes with a step change of its duty cycle reference. The zoomed picture shows that the inductor current response is very fast. The setting time for the capacitor voltage is 1.5 ms for both modes.

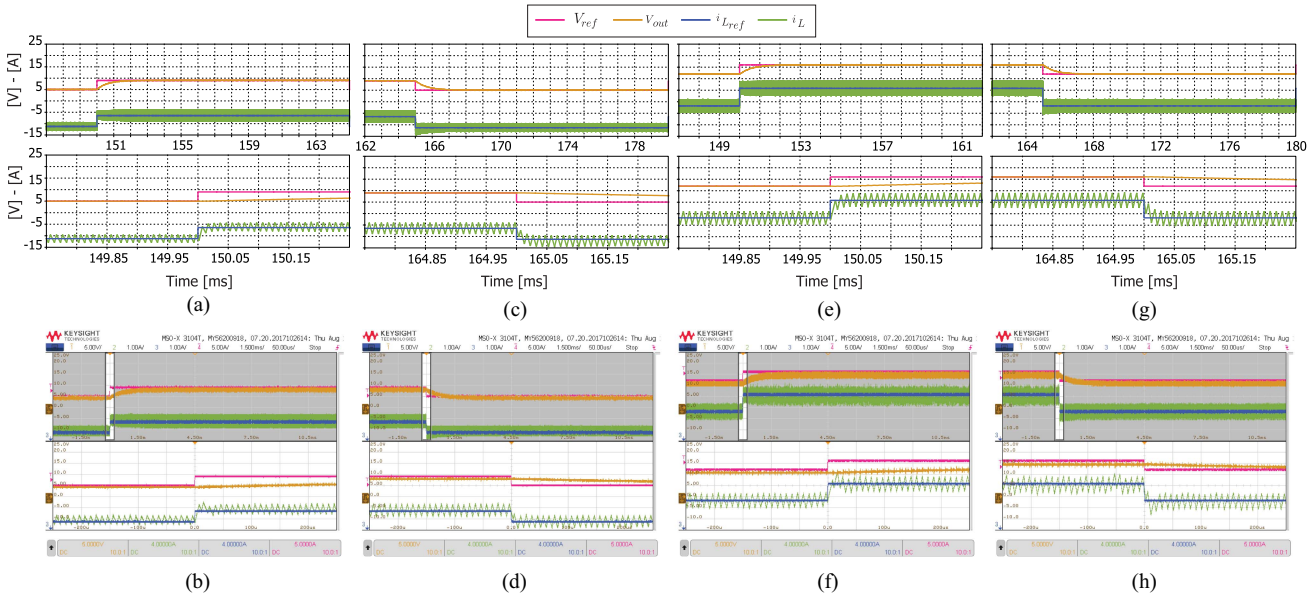

Fig. 5. (a), (c), (e), (g) Simulated and (b), (d), (f), (h) experimental dynamic responses of the buck–boost converter with a load resistance R_L of 10 Ω while the duty cycle reference changes from: (a), (b) 0.33 to 0.47 in buck mode, (c), (d) 0.47 to 0.33 in buck mode, (e), (f) 0.55 to 0.62 in boost mode, and (c), (d) 0.62 to 0.55 in boost mode.

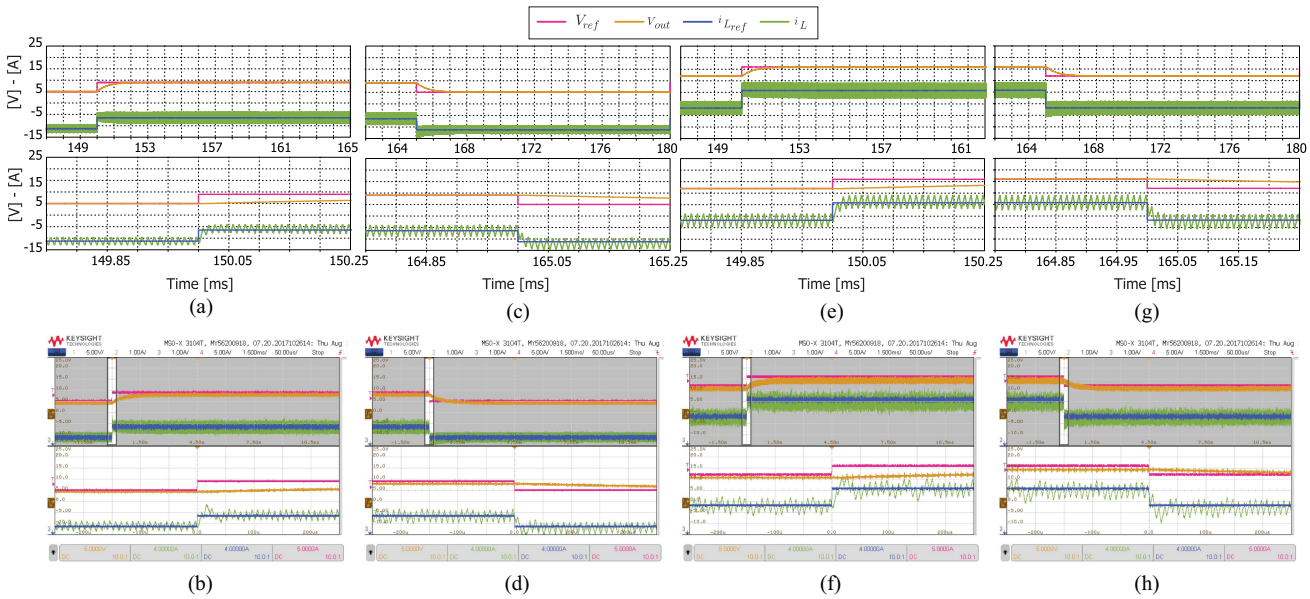

Fig. 6. (a), (c), (e), (g) Simulated and (b), (d), (f), (h) experimental dynamic responses of the noninverting buck–boost converter with a load resistance R_L of 10 Ω while the duty cycle reference changes from: (a), (b) 0.33 to 0.47 in buck mode, (c), (d) 0.47 to 0.33 in buck mode, (e), (f) 0.55 to 0.62 in boost mode, and (c), (d) 0.62 to 0.55 in boost mode.

In addition, the simulated and experimental responses of the noninverting buck–boost converter are shown in Fig. 6. The results demonstrate the effectiveness of the proposed control to regulate all the variables of the converter to achieve a very good tracking performance for both modes and with a setting time for the capacitor voltage of 1.5 ms.

Additional simulation and experimental results were carried out to test the advantages of the proposed control over classic strategies. Fig. 7 compares the proposed CCS-MPC and FCS-MPC regarding computation effort, where 100% represents an

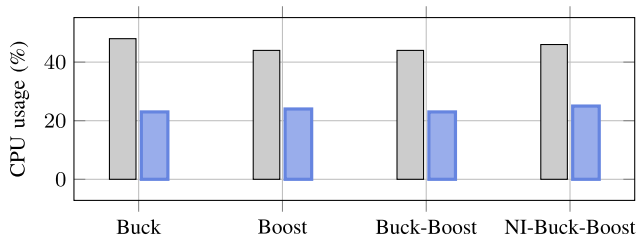

Fig. 7. Comparison in CPU usage between the proposed CCS-MPC (▮▮) and FCS-MPC (▯▯).

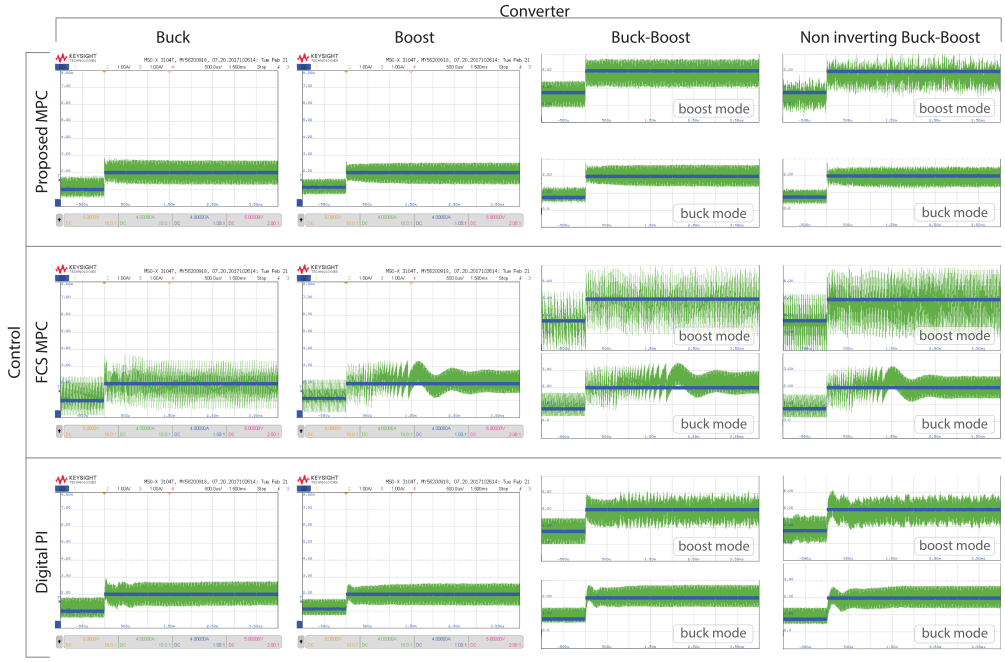

Fig. 8. Experimental dynamic responses using the proposed CCS-MPC, an FCS-MPC, and a digital PI as control.

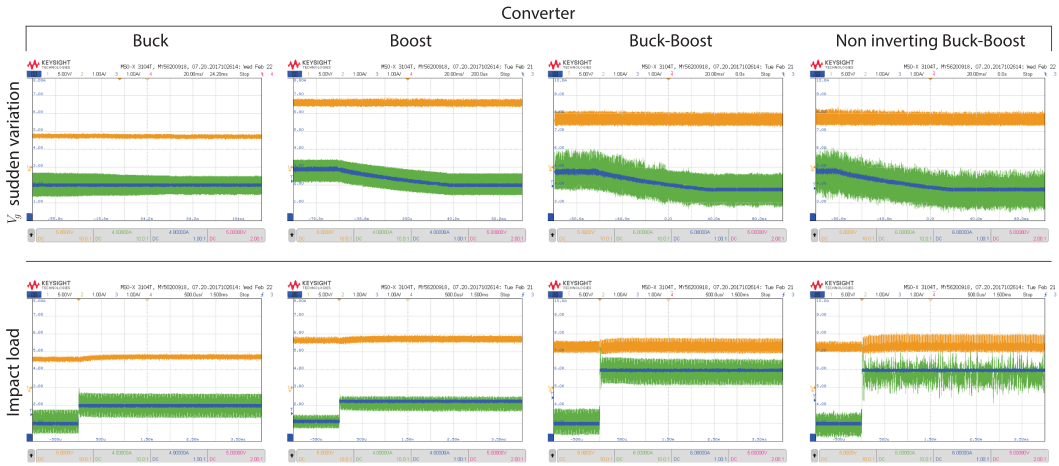

Fig. 9. Experimental dynamic responses for a sudden variation in the input voltage and a variation in the load separately. For the buck converter, V_g dropped from 20 to 15 V, and the impact load varied from 10 to 5 Ω. The V_g of the boost, buck–boost, and noninverting buck–boost converters dropped from 10 to 7 V. The boost converter had an impact load change from 20 to 10 Ω and the buck–boost and noninverting buck–boost converters from 10 to 5 Ω.

entire sampling step. This comparison was obtained by measuring the CPU time in the RT-Box. The proposed CCS-MPC had approximately half the CPU usage of the FCS-MPC. Notice that delay compensation is not required in the proposed CCS-MPC.

Fig. 8 shows an experimental dynamic response of the proposed CCS-MPC strategy, an FCS-MPC, and a digital PI. The proposed CCS-MPC and the digital PI used a sample time of 10 μs, whereas the FSC-MPC used a sample time of 5 μs to match with an equivalent switching frequency of 100 kHz. There was a change in the current for the buck and boost converters from 1 to 2 A. For the buck–boost and noninverting buck–boost converters, buck mode changed from 0.8 to 2 A, and boost mode changed from 3.9 to 5 A. The proposed MPC behaved better than the FCS-MPC, and PI controls under current reference changes for each converter.

Robustness of the proposed control was evaluated by performing abrupt changes in the input voltage or the output load, as shown in Fig. 9. The proposed converter presented an exceptional performance of both output voltage and inductor current despite abrupt disturbances. Fig. 10 shows the mean absolute percentage errors (MAPE) for the proposed control and the FCS-MPC; variations on the capacitance, resistance, and inductance in each of the four converters were considered. The proposed control showed low sensitivity to the converter's parameter variations. In all cases, the control achieved the reference and remained stable.

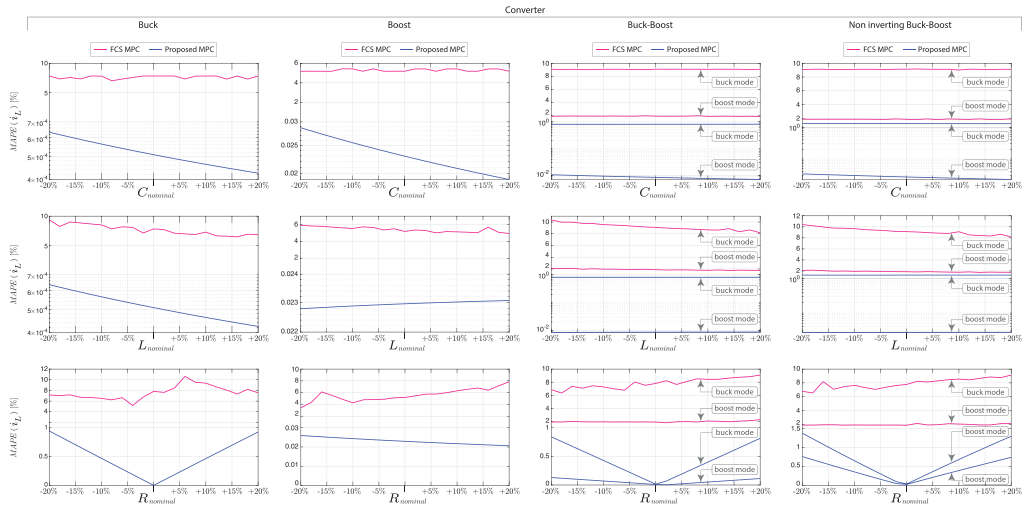

Fig. 10. MAPE of the proposed MPC in comparison with the FCS-MPC when there is variation in the parameters of the converters.

V. Conclusion

A generalized CCS-MPC for second-order dc/dc converters was presented. These converters included the buck, boost, buck–boost, and noninverting buck–boost. The proposed control considered limits in the modulation index as inequality constraints inside the model. The optimization model resulted in a relatively simple equation that could be implemented with a low computational effort. The average CPU utilization of the proposed control and the conventional FCS-MPC was measured. The proposed control showed superior performance.

Simulated and experimental results showed that the proposed control operated at constant frequency with an outstanding performance. The response to a reference change was almost instantaneous in all cases with low overshoot. The proposed control was robust and efficient compared with the conventional FCS-MPC and digital PI controls.

The stability of the control was demonstrated both theoretically and in experimental results. The modulation indices remained within the expected limits, thanks to the inequality restrictions included in the model. The reference was achieved in all cases (i.e., the system is not only stable but also asymptotically stable).

References

[1] S. Vazquez et al., "Model predictive control: A review of its applications in power electronics," *IEEE Ind. Electron. Mag.*, vol. 8, no. 1, pp. 16–31, Mar. 2014, doi: 10.1109/MIE.2013.2290138.

[2] M. E. Albira and M. A. Zohdy, "Adaptive model predictive control for DC-DC power converters with parameters' uncertainties," *IEEE Access*, vol. 9, pp. 135121–135131, 2021.

[3] Q. Xu, Y. Yan, C. Zhang, T. Dragicevic, and F. Blaabjerg, "An offset-free composite model predictive control strategy for DC/DC buck converter feeding constant power loads," *IEEE Trans. Power Electron.*, vol. 35, no. 5, pp. 5331–5342, May 2020.

[4] P. Cortes, M. P. Kazmierkowski, R. M. Kennel, D. E. Quevedo, and J. Rodriguez, "Predictive control in power electronics and drives," *IEEE Trans. Ind. Electron.*, vol. 55, no. 12, pp. 4312–4324, Dec. 2008, doi: 10.1109/TIE.2008.2007480.

[5] P. Karamanakos, T. Geyer, and S. Manias, "Direct voltage control of DC–DC boost converters using enumeration-based model predictive control," *IEEE Trans. Power Electron.*, vol. 29, no. 2, pp. 968–978, Feb. 2014.

[6] C. Bordons and C. Montero, "Basic principles of MPC for power converters: Bridging the gap between theory and practice," *IEEE Ind. Electron. Mag.*, vol. 9, no. 3, pp. 31–43, Sep. 2015, doi: 10.1109/MIE.2014.2356600.

[7] W.-K. Sou, P.-I. Chan, C. Gong, and C.-S. Lam, "Finite-set model predictive control for hybrid active power filter," *IEEE Trans. Ind. Electron.*, vol. 70, no. 1, pp. 52–64, Jan. 2023, doi: 10.1109/TIE.2022.3146550.

[8] M. Aguirre, S. Kouro, C. A. Rojas, and S. Vazquez, "Enhanced switching frequency control in FCS-MPC for power converters," *IEEE Trans. Ind. Electron.*, vol. 68, no. 3, pp. 2470–2479, Mar. 2021, doi: 10.1109/TIE.2020.2973907.

[9] L. Cheng et al., "Model predictive control for DC-DC boost converters with reduced-prediction horizon and constant switching frequency," *IEEE Trans. Power Electron.*, vol. 33, no. 10, pp. 9064–9075, Oct. 2018.

[10] L. Xu, R. Ma, R. Xie, S. Zhuo, Y. Huangfu, and F. Gao, "Offset-free model predictive control of fuel cell DC-DC boost converter with low-complexity and high-robustness," *IEEE Trans. Ind. Electron.*, vol. 70, no. 6, pp. 5784–5796, Jun. 2023, doi: 10.1109/TIE.2022.3198249.

[11] H. Chen, D. Wang, S. Tang, X. Yin, J. Wang, and Z. J. Shen, "Continuous control set model predictive control for three-level flying capacitor boost converter with constant switching frequency," *IEEE Trans. Emerg. Sel. Topics Power Electron.*, vol. 9, no. 5, pp. 5996–6007, Oct. 2021.

[12] A. A. Ahmed, B. K. Koh, and Y. I. Lee, "A comparison of finite control set and continuous control set model predictive control schemes for speed control of induction motors," *IEEE Trans. Ind. Informat.*, vol. 14, no. 4, pp. 1334–1346, Apr. 2018, doi: 10.1109/TII.2017.2758393.

[13] I. Hammoud et al., "On continuous-set model predictive control of permanent magnet synchronous machines," *IEEE Trans. Power Electron.*, vol. 37, no. 9, pp. 10360–10371, Sep. 2022, doi: 10.1109/TPEL.2022.3164968.

[14] C. S. Lim, S. S. Lee, and E. Levi, "Continuous-control-set model predictive current control of asymmetrical six-phase drives considering system non-idealities," *IEEE Trans. Ind. Electron.*, vol. 70, no. 8, pp. 7615–7626, Aug. 2023, doi: 10.1109/TIE.2022.3206703.

[15] Y. Yang et al., "A novel continuous control set model predictive control for LC-filtered three-phase four-wire three-level voltage-source inverter," *IEEE Trans. Power Electron.*, vol. 38, no. 4, pp. 4572–4584, Apr. 2023, doi: 10.1109/TPEL.2023.3233995.

[16] L. Peng, L. Ma, W. Song, and H. Liu, "A simple model predictive instantaneous current control for single-phase PWM converters in stationary reference frame," *IEEE Trans. Power Electron.*, vol. 37, no. 7, pp. 7629–7639, Jul. 2022, doi: 10.1109/TPEL.2022.3141793.

[17] H. T. Nguyen, E.-K. Kim, I.-P. Kim, H. H. Choi, and J.-W. Jung, "Model predictive control with modulated optimal vector for a three-phase inverter with an LC filter," *IEEE Trans. Power Electron.*, vol. 33, no. 3, pp. 2690–2703, Mar. 2018, doi: 10.1109/TPEL.2017.2694049.

[18] H. Zamani, K. Abbaszadeh, J. Gyselinck, and M. Karimi, "Robust continuous control set model predictive control in synchronous reference frame for grid-tied inverters," *IEEE J. Emerg. Sel. Topics Ind. Electron.*, vol. 4, no. 1, pp. 209–218, Jan. 2023, doi: 10.1109/JESTIE.2022.3183474.

[19] B. Ren, Y. Zhu, X. Sun, Z. Pan, and W. Zhao, "Dynamic performance improvement of continuous control set model predictive control for high frequency link matrix converter," *IEEE Trans. Ind. Electron.*, vol. 70, no. 9, pp. 9057–9066, Sep. 2023, doi: 10.1109/TIE.2022.3215447.
[20] L. Cheng et al., "Model predictive control for DC–DC boost converters with reduced-prediction horizon and constant switching frequency," *IEEE Trans. Power Electron.*, vol. 33, no. 10, pp. 9064–9075, Oct. 2018, doi: 10.1109/TPEL.2017.2785255.
[21] M. Sadiq et al., "Continuous-control-set model predictive control for three-level DC–DC converter with unbalanced loads in bipolar electric vehicle charging stations," *Mathematics*, vol. 10, no. 19, 2022, Art. no. 3444.
[22] C. Restrepo, B. Barrueto, D. M.-Yarce, J. Muñoz, E. V.-Idiarte, and R. Giral, "Improved model predictive current control of the versatile buck-boost converter for a photovoltaic application," *IEEE Trans. Energy Convers.*, vol. 37, no. 3, pp. 1505–1519, Sep. 2022.
[23] T. Faulwasser, L. Grune, and M. A. Muller, "Economic nonlinear model predictive control," *Found. Trends Syst. Control*, vol. 5, no. 1, pp. 1–98, 2018, doi: 10.1561/2600000014.
[24] H. T. Nguyen and J.-W. Jung, "Asymptotic stability constraints for direct horizon-one model predictive control of SPMSM drives," *IEEE Trans. Power Electron.*, vol. 33, no. 10, pp. 8213–8219, Oct. 2018, doi: 10.1109/TPEL.2018.2810856.
[25] J. Wang, Y. Tang, P. Lin, X. Liu, and J. Pou, "Deadbeat predictive current control for modular multilevel converters with enhanced steady-state performance and stability," *IEEE Trans. Power Electron.*, vol. 35, no. 7, pp. 6878–6894, Jul. 2020, doi: 10.1109/TPEL.2019.2955485.
[26] Z. Zhang et al., "Advances and opportunities in the model predictive control of microgrids: Part I primary layer," *Int. J. Elect. Power Energy Syst.*, vol. 134, 2022, Art. no. 107411, doi: 10.1016/j.ijepes.2021.107411.
[27] Z. Karami, Q. Shafiee, S. Sahoo, M. Yaribeygi, H. Bevrani, and T. Dragicevic, "Hybrid model predictive control of DC–DC boost converters with constant power load," *IEEE Trans. Energy Convers.*, vol. 36, no. 2, pp. 1347–1356, Jun. 2021.
[28] H. S.-Ramirez and R. Silva-Ortigoza, *Control Design Techniques in Power Electronics Devices*. London, U.K.: Springer, 2006.
[29] M. Grant and S. Boyd, "CVX: Matlab software for disciplined convex programming, version 2.1," Mar. 2014. [Online]. Available: http://cvxr.com/cvx
[30] M. Grant and S. Boyd, "Graph implementations for nonsmooth convex programs," in *Recent Advances in Learning and Control* (Lecture Notes in Control and Information Sciences Series), V. Blondel, S. Boyd, and H. Kimura, Eds. Berlin, Germany: Springer, 2008, pp. 95–110. [Online]. Available: http://stanford.edu/boyd/graph_dcp.html

Alejandro Garcés-Ruiz (Senior Member, IEEE) received the master's degree in electrical engineering from Universidad Tecnológica de Pereira (UTP), Pereira, Colombia, in 2006, and the Ph.D. degree in electrical engineering from the Norges Teknisk Naturvitenskapelige Universitet, Trondheim, Norway, in 2012.

He is currently a Professor with the Department of Electric Power Engineering, UTP.

Dr. Garcés is an Associate Editor for IEEE TRANSACTIONS ON INDUSTRIAL ELECTRONICS and *IET-Renewable Power Generation*. He is also a Member of CIGRE and the Colombian chapter of the Society for Industrial and Applied Mathematics (SIAM). He was the recipient of Georg Forster Research Fellowship for Experienced Researchers from the Alexander Von Humboldt Foundation in Germany in 2020 to continue his research about optimization and control in power systems with inverter-based resources.

Sebastián Riffo was born in Linares, Chile. He received the bachelor's degree in civil engineering in mechatronics in 2021 from the Universidad de Talca, Curicó, Chile, where he is currently working toward the master's degree in engineering sciences with mention in Energy Conversion degree in Faculty of Engineering.

He is part of the Laboratory of Applications in Smart Grids (LARI in Spanish) research group headed by Prof. Carlos Restrepo. His research interests include digital control and dc microgrids.

Catalina González-Castaño received the degree in electronic engineering from the Universidad Nacional de Colombia, Manizales, Colombia, in 2008, the M.Eng. degree in electrical engineering from the Universidad Tecnológica de Pereira, Pereira, Colombia, in 2013, and the Ph.D. (with Hons.) degree in electronic engineering, in the field of power converters for electric vehicles, from the Universitat Rovira i Virgili, Tarragona, Spain, in 2019.

She undertook the Doctoral internship with the Advanced Center of Electrical and Electronic Engineering (AC3E), Valparaiso, Chile. She is currently a Researcher with Energy Transformation Center, Universidad Andres Bello, Santiago, Chile. Her research interests include electric power quality, vehicular power systems, and digital control of power converters.

Carlos Restrepo received the bachelor's (with Hons.) and the master's degrees in electrical engineering from the Universidad Tecnológica de Pereira, Pereira, Colombia, in 2006 and 2007, respectively, and the master's and Ph.D. (with Hons.) degrees in electronic engineering from the Universitat Rovira i Virgili de Tarragona, Tarragona, Spain, in 2008 and 2012, respectively.

He is currently a Professor with the Departamento de Ingeniería Eléctrica, Universidad de Talca, Curicó, Chile. He is also the Director with the Laboratory of Applications in Smart Grids (LARI in Spanish) research group. His research interests include modeling and emulator design for fuel cells, design and digital control of switched converters, and energy management of hybrid electric vehicles.